

University of Nebraska - Lincoln

DigitalCommons@University of Nebraska - Lincoln

Mechanical & Materials Engineering Faculty
Publications

Mechanical & Materials Engineering,
Department of

11-2022

A method of assessing peripheral stent abrasiveness under cyclic deformations experienced during limb movement

Courtney Keiser

Kaspars Maleckis

Pauline Struczewska

Majid Jadidi

Jason N. MacTaggart

See next page for additional authors

Follow this and additional works at: <https://digitalcommons.unl.edu/mechengfacpub>



Part of the [Mechanics of Materials Commons](#), [Nanoscience and Nanotechnology Commons](#), [Other Engineering Science and Materials Commons](#), and the [Other Mechanical Engineering Commons](#)

This Article is brought to you for free and open access by the Mechanical & Materials Engineering, Department of at DigitalCommons@University of Nebraska - Lincoln. It has been accepted for inclusion in Mechanical & Materials Engineering Faculty Publications by an authorized administrator of DigitalCommons@University of Nebraska - Lincoln.

Authors

Courtney Keiser, Kaspars Maleckis, Pauline Struczewska, Majid Jadidi, Jason N. MacTaggart, and Alexey Kamenskiy



HHS Public Access

Author manuscript

Acta Biomater. Author manuscript; available in PMC 2023 January 03.

Published in final edited form as:

Acta Biomater. 2022 November ; 153: 331–341. doi:10.1016/j.actbio.2022.09.044.

A method of assessing peripheral stent abrasiveness under cyclic deformations experienced during limb movement

Courtney Keiser^a, Kaspars Maleckis^b, Pauline Struczewska^b, Majid Jadidi^b, Jason MacTaggart^c, Alexey Kamenskiy^{b,*}

^aDepartment of Mechanical and Materials Engineering, University of Nebraska-Lincoln, Lincoln, NE, United States

^bDepartment of Biomechanics, University of Nebraska Omaha, Biomechanics Research Building, Omaha, NE, United States

^cDepartment of Surgery, University of Nebraska Medical Center, Omaha, NE, United States

Abstract

Poor outcomes of peripheral arterial disease stenting are often attributed to the inability of stents to accommodate the complex biomechanics of the flexed lower limb. Abrasion damage caused by rubbing of the stent against the artery wall during limb movement plays a significant role in reconstruction failure but has not been characterized. Our goals were to develop a method of assessing the abrasiveness of peripheral nitinol stents and apply it to several commercial devices. Misago, AbsolutePro, Innova, Zilver, SmartControl, SmartFlex, and Supera stents were deployed inside electrospun nanofibrillar tubes with femoropopliteal artery-mimicking mechanical properties and subjected to cyclic axial compression (25%), bending (90°), and torsion (26°/cm) equivalent to five life-years of severe limb flexions. Abrasion was assessed using an abrasion damage score (ADS, range 1–7) for each deformation mode. Misago produced the least abrasion and no stent fractures (ADS 3). Innova caused small abrasion under compression and torsion but large damage under bending (ADS 7). Supera performed well under bending and compression but caused damage under torsion (ADS 8). AbsolutePro produced significant abrasion under bending and compression but less damage under torsion (ADS 12). Zilver fractured under all three deformations and severely abraded the tube under bending and compression (ADS 15). SmartControl and SmartFlex fractured under all three deformations and produced significant abrasion due to strut penetration (ADS 20 and 21). ADS strongly correlated with clinical 12-month primary patency and target lesion revascularization rates, and the described method of assessing peripheral stent abrasiveness can guide device selection and development.

Keywords

Abrasion; Stent; Damage; Restenosis; Femoropopliteal artery

*Corresponding author. akamenskiy@unomaha.edu (A. Kamenskiy).

Declaration of Competing Interest

The authors declare that they have no known competing financial interests or personal relationships that could have appeared to influence the work reported in this paper.

1. Introduction

Peripheral Arterial Disease (PAD) often refers to an atherosclerotic obstruction of the femoropopliteal artery (FPA) that reduces blood flow to the lower limbs. Angioplasty with stenting is a minimally invasive procedure to treat PAD, but its clinical outcomes continue to disappoint as a third to a half of the patients develop hemodynamically significant restenosis and require re-intervention within 2–3 years after treatment [1, 2]. While the reasons for these poor clinical results are not entirely clear, the severe biomechanical environment of the lower limb likely plays a central role because it subjects the FPA to significant deformations during limb movement [3–5]. As demonstrated by recent bench-top [6], perfused human cadaver [3], and patient [7, 8] studies, many peripheral stents are unable to accommodate these deformations, resulting in adverse stent-artery interactions that may be responsible for the high restenosis and stent fracture rates in the arteries of the lower extremities [9]. Repetitive locomotion-induced deformations may produce continuous rubbing of the stent against the artery wall, injuring the endothelium, and causing deleterious cellular and biochemical responses that may culminate in disease progression and reconstruction failure [10, 11]. This process may be further exacerbated by stent fractures if sharp metal struts abrade and penetrate the arterial wall, or have little effect if the struts break in a non-abrasive manner [12].

While differences in peripheral stent designs and their biomechanical performances have now been well documented [9], the assessment of their abrasiveness under limb movement-induced FPA deformations remains unexplored. Studies of aortic stent-grafts [13–15] described a method for assessing graft abrasion by the metal stent and demonstrated that laser-cut devices are more aggressive in damaging fabric yarns compared to wire-based stents. Lin et al. [16] suggested that stent-graft abrasion is one of the mechanisms for type V endoleaks and one of the possible causes of Talent stent-graft failure [17], while the study of AneuRx stent-grafts [18] found that 66% of devices had fractures and almost half had at least one hole. These results demonstrate that even aortic wire-based stents that rarely have sharp edges can (and often do) damage the robust graft fabric, pointing to the importance of evaluating this phenomenon in peripheral stents that are often laser-cut [9] and operate in a much more biomechanically hostile environment [3].

The complexity of limb flexion-induced deformations and the highly localized nature of damage do not allow the use of traditional Martindale [14] or Wyzenbeek tests to quantify peripheral stent abrasion. Clinical data can provide indirect evidence, but the variability in patient and lesion characteristics, differences in the applied biomechanical loads that vary with posture and intensity, and the invasive nature of such measurements, make the *in vivo* assessment of stent abrasiveness challenging. The goal of our study was to propose a novel *in vitro* method for assessing stent abrasiveness under well-controlled deformations often experienced by human FPAs. We have developed a reproducible synthetic FPA abrasion model and used it to compare the abrasiveness of seven commercial peripheral stents under axial compression, bending, and torsion deformations equivalent to five life-years of severe limb flexions. The methods and results of this study can be used to guide device selection and the development of novel, less abrasive stents to improve clinical outcomes of endovascular PAD repair.

2. Methods

2.1. Synthetic tubes with FPA-like mechanical properties

Diseased arteries are heterogeneous and cannot survive long-term *ex vivo* testing without degradation. To circumvent these issues, we have manufactured 6mm synthetic tubes with FPA-like mechanical properties by electrospinning polyurethane Pellethane (The Lubrizol Corporation) 5863–82A (PU 82A) at 10% weight/weight and 2% of the polymer mass of Coomassie Brilliant Blue R-250 dissolved in 6:4 weight/weight tetrahydrofuran and dimethylformamide solvents (both MilliporeSigma), respectively. A conductive collector rod wrapped with 24-gauge copper wire was used to aid in the removal of the tubes. The polymer solution was loaded into a 10 mL plastic syringe (CareTouch) with a 25-gauge blunt tip and 1” Luer lock needles, and mounted onto a syringe pump (Chemyx Fusion 200) set on a linear translational stage (ASHANKS Shenzhen DsIrk Technology Co). The PU nanofibrillar tube was electrospun on top of the copper wire at a rate of 2 ml/h for 2 h at a 20 kV potential difference. The working distance between the collector rod and the syringe pump was 12 cm, and the travel distance of the linear translational stage was 45 cm at a speed of 2.8 cm/s. The graft thickness was controlled by adjusting the total solution feed volume during electrospinning. Tubes were made at an initial length of 45 cm (removing 4–5 cm from each end) and cut into 5 cm-long segments to accommodate 4 cm long stents. Every fifth 45 cm graft was used to perform a quality check by sectioning the tube in 1 cm increments and measuring thickness under a Leica MZ75 stereomicroscope. The average thickness of the nanofibrillar tubes was $127.1 \pm 6.6 \mu\text{m}$. Using the CellScale Biotester (CellScale, Ontario, Canada) and the experimental protocols described previously [19–22], we have evaluated the mechanical stiffness of our tubes and have adjusted the electrospinning manufacturing parameters to match the circumferential stiffness of > 70-year-old human FPAs in the 50th percentile (i.e., 954 kPa) [20]. Axial, torsional, and bending stiffnesses of the tube were considered negligible, because in unpressurized FPAs they are much lower than those of stents [6]. The resulting nanofibrous tubes were subjected to equibiaxial mechanical testing, and their Young’s modulus was $929 \pm 11 \text{ kPa}$ calculated from the engineering circumferential stress-strain data at 10% strain, which was not statistically different from that of the old human FPAs (954 kPa, $p = 0.13$) [20]. The synthetic abrasion model was validated by comparing its stent-induced damage with that produced by the same devices deployed in human FPAs as described in the next section.

2.2. Comparison of the nanofibrillar tubes to human FPA

The ability of the nanofibrillar tubes to simulate stent-induced damage was verified by comparing the results to those obtained with the same type of stents deployed in real human FPAs. Fig. 1(A) demonstrates a Smart Control (Cordis) stent deployed into an *ex vivo* human FPA, and Fig. 1 (B,C) demonstrates the result of subjecting the artery to cyclic torsional deformations that fractured the stent and resulted in its struts penetrating the artery wall. Despite the faint imprint that can be seen in Fig. 1(C), it was not possible to accurately and repeatedly quantify this abrasion, which stimulated the development of a repeatable synthetic vessel approach.

2.3. Stents

Seven stents frequently used to treat PAD (Fig. 2) were used in the analysis. These included AbsolutePro and Supera (Abbott Vascular), Innova (Boston Scientific), Zilver (Cook Medical), SmartControl and SmartFlex (Cordis), and Misago (Terumo). All stents except Supera had a 7 mm diameter to account for the 1 mm oversizing recommended by the manufacturers. The diameter of Supera was 6 mm to allow 1:1 sizing required by the manufacturer. Stent geometry and strut profiles were analyzed using microcomputed tomography (μ CT) and an EasyTom S 150 (Productivity Quality, Inc., Plymouth, MN) scanner with a copper filter. Scans were done at 5.86 μ m voxel size, 150 kV voltage, 66 μ A current, a frame rate of 5, and the number of frames set at 7. Three-dimensional reconstructions were done using Mimics v24 software (Materialize, Leuven, Belgium), and the analysis was done in 3-Matic v16 software (Materialize, Leuven, Belgium). Stent strut thickness, strut width, inner and outer strut roundness (fillets), smallest and largest apices, and the total number of apices in the cross-section were measured for each device. The measurements were done at nine different locations and averaged. The inner and outer fillets and the sharpness of the apices were quantified by fitting circles and recording their radii. After imaging, the stents were deployed into the nanofibrillar tubes and mechanically tested under axial compression, bending, and torsion deformations.

2.4. Mechanical testing

Stent segments 4 cm long were crimped onto a delivery catheter, deployed into 5 cm long nanofibrillar tubes (Fig. 3A), attached to custom-built fixtures (Fig. 3B–D) by clamping the stent on both ends, and evaluated under displacement-controlled axial compression, bending, and torsion deformations at 37°C for a total of 345,600 cycles at 2 Hz using the TA Electroforce 5175 BioDynamic tester (New Castle, DE, USA). Tubes were not pressurized because the permeability of the material, abrasion, and strut penetration did not allow to maintain stable pressure. Values of axial compression (25%), bending (90°), and torsion ($\pm 26^\circ$ /cm rotation) were determined previously [3–5, 9] and represented the worst-case fetal/gardening posture. In a single day, patients with affected lower extremities bend their limbs to this position ~ 180 times [23], and therefore 345,600 cycles represented ~ 5 life-years worth of limb flexions, while the 5-year PAD patient mortality is $\sim 50\%$ [24]. Because of the significant rate of stent fracture, one stent was used per deformation mode.

2.5. Quantification of abrasion

Abraded nanofibrillar tubes were imaged and characterized using Scanning Electron (SEM) and optical microscopy. Electrospun tubes were coated with gold using a Cressington sputter coater for 15 s prior to imaging. An FEI Helios NanoLab 660 scanning electron microscope was used for imaging using voltages between 2 and 5 kV. Stents were imaged using an SNE-4500M Plus Table-top SEM using voltages between 10 and 15 kV. Optical microscopy of the abraded tubes was done using the Leica MZ75 stereomicroscope at 2.0x magnification and Nikon D5200 digital camera. The non-abraded and abraded segments of the nanofibrillar fabric were traced manually in an image analysis software (ImageJ), as shown in Fig. 4.

For each device and each deformation mode, the Abrasion Ratio (AR) defined as the area of the abraded region to the area of the corresponding non-abraded region, was measured. The non-abraded segment was taken from the area where the stent was clamped into the fixture, creating an imprint in the nanofibrillar fabric that was traced manually in an image analysis software (ImageJ). For consistency, five different unit cells containing one complete stent apex were measured in each sample, and the results were averaged. Tracing was performed twice by the same operator in random order, and the error was similar to tracing different unit cells of the same stent. If the stent abrasion was the same or less than the stent imprint area, the stent was assigned an AR of 1.0, indicating little interaction between the stent and the tube.

In addition to the AR, a semi-quantitative additive scoring system was used to assess the overall abrasion damage score (ADS) for each device and each deformation mode. A small amount of abrasion resulting from the minimal interaction between the stent and the tube ($AR < 2$) added +1 to the score, while medium abrasion ($2 \leq AR < 3$) added +2, and severe abrasion with extensive wear ($AR \geq 3$) added +3. In addition, if the stent had broken struts, the ADS increased by +1, and if the broken struts tore through the tube fabric, the score increased by +3. ADS was added across deformation modes and compared across devices.

2.6. Statistical analysis

Pearson (r) and Spearman (ρ) coefficients were calculated to assess the strength of correlation between the abrasion ratio, stent design characteristics measured using μ CT, device stiffness [6], and clinical primary patency rates. The strength and statistical significance of correlations were assessed using Matlab's *corr* function by testing the hypothesis of no correlation against the alternative that there is a nonzero correlation assuming statistical significance at $p < 0.05$.

3. Results

3.1. Abrasion under axial compression

Misago, AbsolutePro, Innova, and Supera accommodated 25% axial compression without fractures, while Zilver, SmartControl, and SmartFlex had various degrees of strut fracture or complete stent separation. Images of the abraded tubes (Fig. 5) demonstrate the effect of stent design on abrasion severity, and ARs are summarized in Table 1. SmartFlex produced the most abrasion (AR 4.07) and had ten broken struts (+1 ADS) that tore through the fabric (+3 ADS), resulting in an ADS of 7. SmartControl had an AR of 3.25 (+3 ADS), broke in half during testing (+1 ADS), and the sharp strut edges tore holes through the tube (+3 ADS), resulting in an ADS of 7. Zilver produced moderate abrasion (AR 2.79, +2 ADS), but had three strut fractures (+1 ADS) that tore through the fabric (+3 ADS), adding to an ADS of 6. AbsolutePro had an AR of 2.11 (+2 ADS), and its single-prong apexes abraded the tube more than its three-prong apexes. Though the struts had no fractures (+0 ADS), the stent wore through the fabric (+3 ADS), producing holes and resulting in an ADS of 5. Innova, Misago, and Supera caused the least abrasion (Innova AR 1.97, Misago AR 1.33, Supera AR 1.0, for all +1 ADS), did not have strut fractures (+0 ADS), or fabric penetrations (+0 ADS), and all had ADS of 1.

3.2. Abrasion under bending

Misago and Supera were the only stents able to accommodate 90° bending without fractures or tearing through the fabric, while AbsolutePro, Innova, Zilver, SmartControl, and SmartFlex had various degrees of strut fracture. Fractures typically occurred along the inner curve of the bend where the stents compressed and their struts tended to tangle. Abraded tube images are presented in Fig. 6, while the ARs are summarized in Table 1. SmartControl (AR 3.65), SmartFlex (AR 3.60), and Zilver (AR 3.31) produced the most abrasive interaction with the tube (+3 ADS). SmartControl had 8 broken struts (+1 ADS), SmartFlex had 6 broken struts (+1 ADS), and Zilver had 2 broken struts (+1 ADS) that aggressively abraded the fabric (+3 ADS), causing multiple tears. Each of these stents received an ADS of 7. AbsolutePro had an AR of 2.26 (+2 ADS) with 2 strut fractures (+1 ADS) that penetrated the tube (+3 ADS) and resulted in an ADS of 6. Innova (AR 1.86) caused mild abrasion (+1 ADS) but experienced two strut fractures (+1 ADS) pierced that through the fabric (+3 ADS), producing an ADS of 5. Misago and Supera caused the least abrasion (Misago AR 1.31, Supera AR 1.0) with no strut fractures (+0 ADS) or tube penetrations (+0 ADS), and both had an ADS of 1.

3.3. Abrasion under torsion

Misago, AbsolutePro, and Innova accommodated 26°/cm twists without fractures, while Zilver, SmartControl, SmartFlex, and Supera fractured to various degrees. Abraded tube images are presented in Fig. 7, and ARs are summarized in Table 1. SmartFlex produced the most severe abrasion (AR 4.18, +3 AD) and had 3 broken struts (+1 ADS) that penetrated the tube (+3 ADS), resulting in an ADS of 7. SmartControl had an AR of 2.61 (+2 ADS) and broke in half (+1 ADS). Its struts produced holes (+3 ADS) which added to an ADS of 6. Supera also broke in half (+1 ADS), and its exposed wires tore the tube (+3 ADS). The AR for Supera was 2.47 (+2 ADS), and an ADS was 6. Zilver had an AR of 1.42 (+1 ADS) and three strut fractures (+1 ADS), but the fractured struts did not produce holes (+0 ADS), and an ADS was 2. AbsolutePro (AR 1.82), Innova (AR 1.62), and Misago (AR 1.40) caused the least abrasion with no strut fractures (+0 ADS) or fabric penetration (+0 ADS), and all scored an ADS of 1.

3.4. Influence of stent design parameters on abrasion

Stent strut profile characteristics and device stiffnesses under axial compression, bending, and torsion [6] are summarized in Table 1. Abrasion under compression had positive correlation with the number of stent apices ($r = 0.8$, $p = 0.04$, $R^2 = 0.59$, Fig. 8A) and the stiffness of in the stent compression ($r = 0.9$, $p = 0.004$, $R^2 = 0.84$, = Fig. 8B while strut thickness ($p = 0.82$), width ($p = 0.26$), inner fillet ($p = 0.13$), outer fillet ($p = 0.12$), fillet and apex ($p = 0.34$) did not have statistically significant effects on the Abrasion Ratio (AR). Stent's torsional stiffness also did not affect abrasion under compression ($p = 0.25$), but there was a positive (although not statistically significant, $p = 0.10$) trend with the stent's bending stiffness ($r = 0.66$).

Abrasion under cyclic bending exhibited positive correlation with the compressive stiffness of the stent ($r = 0.9$, $p < 0.01$, $R^2 = 0.8$, Fig. 8C), while the effects of strut thickness ($p = 0.71$), width ($p = 0.25$), inner fillet ($p = 0.14$), outer fillet ($p = 0.15$), fillet and

apex ($p = 0.37$) were not significant. Stents with more apices produced greater abrasion during bending ($r = 0.7$), but this result was not statistically significant ($p = 0.07$). Stent's bending stiffness also did not affect abrasion under bending ($p = 0.23$), but torsional stiffness appeared to have a somewhat positive, although not statistically significant, effect ($r = 0.7$, $p = 0.06$).

Abrasion under torsion was not significantly influenced by any of the stent profile ($r = -0.32$ to -0.45 , and $p = 0.32$ – 0.99) or device stiffness ($r = 0.17$ – 0.71 and $p = 0.07$ – 0.71) characteristics, although there was a positive trend with the compressive stent stiffness ($r = 0.71$) that did not reach statistical significance ($p = 0.07$).

4. Discussion

PAD stents are metal tubes implanted into delicate arteries, interacting with them daily with each limb movement. Significant efforts are put into understanding this interaction by quantifying stresses, deformations, and flow [3, 6, 8], but no attention has yet been given to abrasion resulting from this interplay. In this study, we have developed a method to assess PAD stent abrasiveness using synthetic artery-mimicking nanofibrillar tubes and compared the performance of 7 commercial devices over five life-years of severe limb flexions. Our data demonstrate (Fig. 9) that of all analyzed stents, Misago could withstand deformations without fractures and had the lowest cumulative ADS of 3. Clinically, Misago has one of the highest 12-month primary patency rates (88%, Table 1) reported by a large 744-patient MISAGO-2 study [25]. In bench-top testing, Misago demonstrated the smallest compression and bending stiffness of all 7 devices, and had the second smallest number of apices – the characteristics that likely contributed to less abrasion. Innova also produced minimum abrasion during compression and torsion but caused significant damage during bending because of its fractured struts (ADS 7). Clinically, Innova had an 86% primary patency rate at 12 months [27] and a 2% fracture rate. Supera had the third-lowest cumulative ADS of 8, but the lowest AR of all stents under compression and bending, possibly because it was the only stent that was not oversized. Under torsion, however, Supera fractured, and its wires penetrated the tube. Clinically, Supera fractures are rare [33], but have been reported [34, 35], which points to the limitation of applying the same displacement-controlled boundary conditions to all stents. The *in vivo* loading environment likely includes a combination of force-controlled (pressure from the surrounding tissues and muscles) and displacement-controlled (pulling of side branches and flexion at the joint) conditions, although the exact contribution of each is currently unknown. A human cadaver model that evaluated the effects of stents on limb flexion-induced deformations [3] reported a 47% restriction of twist in the stented segment for the Supera stent and a 59% exacerbation of twist distal to the stent. Nevertheless, we have applied the same loading conditions to all stents because the amount of restriction/exacerbation observed in cadavers was device-specific and not measured for all stents evaluated in the current study. This is a clear limitation that should be addressed with future research. Despite this experimental shortcoming, the abrasion data for Supera are in good agreement with its clinical performance [33] and the reported 12-month primary patency of 68–88% (average 81%).

The remaining four stents caused significant abrasion under more than one deformation mode. AbsolutePro wore through the tube under compression and tore the fabric during bending, resulting in a cumulative ADS of 12. The 12-month primary patency of AbsolutePro is 80% [26]. The abrasion performance of the Zilver was similar, with the second-lowest AR under torsion (despite the broken struts that did not tear through the tube), but worse performance under compression and bending, which produced a cumulative ADS of 15. Clinically, the bare-metal Zilver has a 73% primary patency rate at 12 months [28], and the paclitaxel-coated Zilver PTX has a 75% patency [36]. The two stents that caused the most abrasion were SmartControl and SmartFlex, scoring 20 and 21 on an ADS, respectively. These stents demonstrated the most fractured struts and tore through the tube under all three deformations. The patency rate of the SmartControl ranges from 46% [29] to 71% [30] (average 62%), and SmartFlex 12-month primary *assisted* patency is 83% [31]. While the *unassisted* patency of SmartFlex was not specified, another study [32] reported a 62% freedom from target lesion revascularization (TLR) at 12 months despite the assisted primary patency of 92%. In a cadaver model [3], SmartControl and SmartFlex stents significantly influenced natural limb flexion-induced deformations, and in bench-top tests [6], they had higher stiffness compared to other devices. SmartControl and SmartFlex also had the largest number of apexes, and this design feature, along with the high compression and bending stiffness of these devices, likely contributed to more severe abrasion. These data suggest that the inability of the stent to accommodate limb flexion-induced deformations may result in significant interaction with the artery wall, which may produce greater abrasion and potentially lead to the loss of patency. Spearman correlation between AD and the 12-month primary patency rates reported in Table 1 were -0.64 ($p = 0.14$), but when using the TLR rate of 62% for the SmartFlex instead of its 83% primary assisted patency (loss of patency is often the main reason for TLR), the correlation becomes -0.99 ($p < 0.01$). Despite the strong correlation, it should be interpreted with care because clinical data are significantly influenced by patient selection, demographics, lesion characteristics, calcification, stent overlap, and other parameters that affect patency. Large variation in results for the same devices suggests that a meta-analysis controlling for these conditions is warranted to perform a proper comparison, and perhaps it can be informed by the presented data on stent abrasiveness.

Abrasion damage appears particularly relevant in light of recent clinical data from paclitaxel-loaded PAD stents. Patients treated with a polymer-coated Eluvia had a prolonged release of paclitaxel and a 13% loss of primary patency at 12 months, which is not much better than the 86% primary patency of its non-drug-coated Innova [27] platform. But 8% of the Eluvia-treated arteries also developed aneurysms that were attributed to the drug [37], transforming patients in stable condition into those requiring closer surveillance for possible higher thrombotic and bleeding risks. While the mechanism of how paclitaxel promotes the development of aneurysms has not been identified [37, 38], our current analysis suggests that it could be related to the mechanical abrasion that fails to heal under the prolonged suppressive effects of the drug. Paclitaxel is an inhibitor of the vascular smooth muscle cell and fibroblast proliferation, migration, and secretion of the extracellular matrix, which are all hallmarks of tissue damage repair. Large animal studies [39] have demonstrated that slow paclitaxel release of the Eluvia stent (> 300 days) produced a greater propensity to

aneurysmal degeneration compared with the rapid (< 60 days) drug release by the Zilver PTX.

While our study presents the first attempt to evaluate the abrasiveness of lower extremity stents, points to the importance of minimizing abrasive interaction between the stent and the artery wall during limb movement-induced deformations, and suggests that the reported results agree well with clinical evidence of arterial patency, we need to stress its limitations. First, while bench-top tests provide precise control of the loading conditions, they do not fully recapitulate the complexity of the *in vivo* environment with its combined mix-mode loading, pressurization, biological repair mechanisms, and other factors that are difficult to simulate *in vitro*. The mixture of force-controlled and displacement-controlled loading conditions that stem from the influence of the surrounding tissues, side branches, and flexion at the joint is particularly complex. The displacement-controlled conditions appear to be dominant in axial compression and bending, while torsion may be more affected by muscle interactions rather than the geometric effects of the joint. Because of the lack of force-controlled data, our experiments were purely displacement-controlled, and this likely resulted in harsher loading conditions for some stents, such as Supera. Similarly to displacement-controlled tests, force-controlled experiments have their own limitations. For example, the loss of structural integrity due to strut fracture may result in greater deformations when the same forces continue to be applied during the test, producing inconsistent loading rates and potentially unrealistically high deformations. Perhaps a displacement-controlled test with device-specific amplitudes would be a better alternative, but future studies are needed to determine these conditions for different stents. This will also be challenging for the new device prototypes that have not yet been implanted into an anatomically accurate environment to assess their effects on natural limb movement-induced deformations.

Second, we have used one stent for each test because cyclic loading experiments are lengthy, expensive, and have high rates of device failure. Studies with a larger number of stents are warranted, even though commercial devices pass rigorous quality checks which minimize the expected variability. Importantly, we also evaluated only one stent length (4cm) because it was the maximum allowed by our testing equipment to support 25% axial compression. Longer stents may produce different abrasion and require additional external support to avoid buckling during the test. To minimize the influence of stent length on the results, our AR metric normalized the abraded area to the non-abraded area.

Third, while our nanofibrillar tubes mimicked the mechanical properties of human FPAs, they did not have plaques that may affect stent behavior. Atherosclerotic plaques are heterogeneous, and the construction of such models requires comprehensive parametric assessments that will be the focus of future studies.

Fourth, we applied harsh loading conditions to stents. These deformations were equivalent to five life-years of severe limb flexions and evaluated the worst-case loading scenario. Furthermore, the displacement-based loading conditions were based on non-stented arteries, which in general are more severe than those of the stented vessels [3]. Additional studies are needed to assess the influence of load range and the number of cycles on abrasive damage.

Subjecting stents to the worst-case deformations sets a high bar for their performance. Prior studies have reported lower values of limb flexion-induced deformations [40–44] when averaged over longer arterial segments, and a detailed discussion of the differences in the measurement techniques is provided elsewhere [9, 45]. Importantly, the presented methodology of assessing stent abrasiveness can be used with milder loading, such as that occurring during walking or stair climbing. Device evaluation at different cycle counts would also be interesting as it would demonstrate the effect of isolated early fractures on abrasion. Because abrasion is a function of stent design, material, surface finish, and other parameters, not all fractures are likely to result in severe abrasion, and likewise, the absence of strut fractures may not necessarily mean less abrasion.

Fifth, we have sized stents according to their manufacturer recommendations, but this may not always be the case clinically. In a pilot study, we investigated the effect of stent under- and oversizing, and while we did not have all devices in all diameters subjected to all deformation modes, our results suggest that the trends across stents generally remained similar, with Misago, Innova, and Supera producing less abrasion than other devices. We have also observed worse abrasion with larger oversizing, likely due to more interaction between the stent and the tube, but future studies should evaluate these effects in greater detail.

Sixth, we have not investigated friction between the stent and the tube, although it is likely different than between the stent and the artery in either dry or wet conditions. Frictional characteristics of arteries are poorly understood [46] due to the difficulty of experimental measurements and the influence of patient characteristics. Stent friction depends on specific design and surface finish and is also not trivial to assess. But regardless of friction, a qualitative comparison of abrasion pattern and severity between a human FPA and our nanofibrous tube (Fig. 1C and D) suggests that the tube provides a reasonable approximation of abrasion occurring in arteries. Additional validation comparing abrasion in native arteries and nanofibrillar tubes under all modes of deformation is warranted.

Lastly, though we have only assessed seven stent designs, the proposed methodology can in the future be used to compare any number of peripheral stents, possibly making the AR and ADS metrics standard for device manufacturers.

Acknowledgments

This work was supported in part by the NIH awards HL125736, HL147128, and AG062198.

Data availability

Data will be made available from the corresponding author upon a reasonable request.

References

- [1]. Stavroulakis K, Torsello G, Manal A, Schwindt A, Hericks C, Stachmann A, Schönefeld E, Bisdas T, Results of primary stent therapy for femoropopliteal peripheral arterial disease at 7 years, *J. Vasc. Surg* 64 (2016) 1696–1702, doi: 10.1016/j.jvs.2016.05.073. [PubMed: 27575816]

- [2]. Qato K, Conway AM, Mondry L, Giangola G, Carroccio A, Management of isolated femoropopliteal in-stent restenosis, *J. Vasc. Surg* 68 (2018) 807–810, doi: 10.1016/j.jvs.2018.01.030. [PubMed: 30144908]
- [3]. MacTaggart J, Poulson W, Seas A, Deegan P, Lomneth C, Desyatova A, Maleckis K, Kamenskiy A, Stent design affects femoropopliteal artery deformation, *Ann. Surg* 270 (2019) 180–187, doi: 10.1097/SLA.0000000000002747. [PubMed: 29578912]
- [4]. Poulson W, Kamenskiy A, Seas A, Deegan P, Lomneth C, MacTaggart J, Limb flexion-induced axial compression and bending in human femoropopliteal artery segments, *J. Vasc. Surg* 67 (2018) 607–613, doi: 10.1016/j.jvs.2017.01.071. [PubMed: 28526560]
- [5]. Desyatova A, Poulson W, Deegan P, Lomneth C, Seas A, Maleckis K, MacTaggart J, Kamenskiy A, Limb flexion-induced twist and associated intramural stresses in the human femoropopliteal artery, *J. R. Soc. Interface* 14 (2017) 20170025, doi: 10.1098/rsif.2017.0025.
- [6]. Maleckis K, Deegan P, Poulson W, Sievers C, Desyatova A, MacTaggart J, Kamenskiy A, Comparison of femoropopliteal artery stents under axial and radial compression, axial tension, bending, and torsion deformations, *J. Mech. Behav. Biomed. Mater* 75 (2017) 160–168, doi: 10.1016/j.jmbbm.2017.07.017. [PubMed: 28734257]
- [7]. Spinella G, Finotello A, Pane B, Salsano G, Mambrini S, Kamenskiy A, Gazzola V, Cittadini G, Auricchio F, Palombo D, Conti M, *In vivo* morphological changes of the femoropopliteal arteries due to knee flexion after endovascular treatment of popliteal aneurysm, *J. Endovasc. Ther* 26 (2019), doi: 10.1177/1526602819855441.
- [8]. Gökçöl C, Diehm N, Räber L, Büchler P, Prediction of restenosis based on hemodynamical markers in revascularized femoro-popliteal arteries during leg flexion, *Biomech. Model. Mechanobiol* (2019), doi: 10.1007/s10237-019-01183-9.
- [9]. Maleckis K, Anttila E, Aylward P, Poulson W, Desyatova A, MacTaggart J, Kamenskiy A, Nitinol stents in the femoropopliteal artery: a mechanical perspective on material, design, and performance, *Ann. Biomed. Eng* 46 (2018), doi: 10.1007/s10439-018-1990-1.
- [10]. Kearney M, Pieczek A, Haley L, Losordo DW, Andres V, Schainfeld R, Rosenfield K, Isner JM, Histopathology of in-stent restenosis in patients with peripheral artery disease, *Circulation* 95 (1997) 1998–2002, doi: 10.1161/01.cir.95.8.1998. [PubMed: 9133506]
- [11]. Chaabane C, Otsuka F, Virmani R, Bochaton-Piallat ML, Biological responses in stented arteries, *Cardiovasc. Res* 99 (2013) 353–363, doi: 10.1093/cvr/cvt115. [PubMed: 23667187]
- [12]. Babaev A, Hari P, Zavrunova S, Kurayev A, Role of nitinol stent fractures in the development of in-stent restenosis in the superficial femoral artery, *Vasc. Dis. Manag* 13 (2016) 7–16.
- [13]. Yao T, Choules BD, Rust JP, King MW, The development of an *in vitro* test method for predicting the abrasion resistance of textile and metal components of endovascular stent grafts, *J. Biomed. Mater. Res. Part B Appl. Biomater* 102 (2014) 488–499, doi: 10.1002/jbm.b.33026
- [14]. Rodrigues A, Figueiredo L, Bordado J, Abrasion behaviour of polymeric textiles for endovascular stent-grafts, *Tribol. Int* 63 (2013) 265–274, doi: 10.1016/j.triboint.2012.11.003.
- [15]. Lin J, Nutley M, Li C, Douglas G, Du J, Zhang Z, Douville Y, Guidoin R, Wang L, Innovative textile structures designed to prevent type III endoleaks in endovascular stent-grafts, *Artif. Organs* 45 (2021) 278–288, doi: 10.1111/aor.13819. [PubMed: 32969519]
- [16]. Lin J, Guidoin R, Du J, Wang L, Douglas G, Zhu D, Nutley M, Perron L, Zhang Z, Douville Y, Lin J, Guidoin R, Du J, Wang L, Douglas G, Zhu D, Nutley M, Perron L, Zhang Z, Douville Y, An *in vitro* twist fatigue test of fabric stent-grafts supported by Z-stents vs. ringed stents, *Materials* 9 (2016) 113, doi: 10.3390/ma9020113. [PubMed: 28787913]
- [17]. Lin J, Guidoin R, Wang L, Zhang Z, Nutley M, Paynter R, Wei D, How T, Crépeau H, Douville Y, Samis G, Dionne G, Gilbert N, Fatigue and/or failure phenomena observed in the fabric of stent-grafts explanted after adverse events braided stent-grafts view project design, fabrication AND evaluation of polymeric bioresorbable cardiovascular stent view project fatigue and/or failure, *Artic. J. Long Term Eff. Med. Implant* 23 (2013) 67–86, doi: 10.1615/JLongTermEffMedImplants.2013007769.
- [18]. Zarins CK, Arko FR, Crabtree T, Bloch DA, Ouriel K, Allen RC, White RA, Explant analysis of AneuRx stent grafts: relationship between structural findings and clinical outcome, *J. Vasc. Surg* 40 (2004) 1–11, doi: 10.1016/J.JVS.2004.03.008. [PubMed: 15218454]

- [19]. Jadidi M, Desyatova A, MacTaggart J, Kamenskiy A, Mechanical stresses associated with flattening of human femoropopliteal artery specimens during planar biaxial testing and their effects on the calculated physiologic stress-stretch state, *Biomech. Model. Mechanobiol* 18 (2019) 1591–1605, doi: 10.1007/s10237-019-01162-0. [PubMed: 31069592]
- [20]. Jadidi M, Razian SA, Anttila E, Doan T, Adamson J, Pipinos M, Kamenskiy A, Comparison of morphometric, structural, mechanical, and physiologic characteristics of human superficial femoral and popliteal arteries, *Acta Biomater* 121 (2021) 431–443, doi: 10.1016/j.actbio.2020.11.025. [PubMed: 33227490]
- [21]. Jadidi M, Razian SA, Habibnezhad M, Anttila E, Kamenskiy A, Doan T, Adamson J, Pipinos M, Kamenskiy A, Habibnezhad M, Anttila E, Kamenskiy A, Mechanical, structural, and physiologic differences in human elastic and muscular arteries of different ages: Comparison of the descending thoracic aorta to the superficial femoral artery, *Acta Biomater* 119 (2021) 268–283, doi: 10.1016/j.actbio.2020.10.035. [PubMed: 33127484]
- [22]. Kamenskiy A, Seas A, Deegan P, Poulson W, Anttila E, Sim S, Desyatova A, MacTaggart J, Constitutive description of human femoropopliteal artery aging, *Biomech. Model. Mechanobiol* 16 (2017) 681–692, doi: 10.1007/s10237-016-0845-7. [PubMed: 27771811]
- [23]. Wimmer MA, Nechtow W, Schwenke T, Moisio KC, Knee Flexion and daily activities in patients following total knee replacement: a comparison with ISO standard 14243, *Biomed Res. Int* 2015 (2015), doi: 10.1155/2015/157541.
- [24]. Feringa HHHH, Bax JJ, Hoeks S, van Waning VH, Elhendy A, Karagiannis S, Vidakovic R, Schouten O, Boersma E, Poldermans D, Van Waning VH, Elhendy A, Karagiannis S, Vidakovic R, Schouten O, Boersma E, Poldermans D, A prognostic risk index for long-term mortality in patients with peripheral arterial disease, *Arch. Intern. Med* 167 (2007) 2482–2489, doi: 10.1001/archinte.167.22.2482. [PubMed: 18071171]
- [25]. Schulte KL, Kralj I, Gissler HM, Bagnaschino LA, Buschmann I, Pernès JM, Haage P, Goverde P, Beregi JP, Válka M, Boudny J, Geibel T, Velkoborsky M, Zähringer M, Paetzel C, Fanelli F, Müller-Hülsbeck S, Zeller T, Langhoff R, MISAGO 2: one-year outcomes after implantation of the Misago self-expanding nitinol stent in the superficial femoral and popliteal arteries of 744 patients, *J. Endovasc. Ther* 19 (2012) 774–784, doi: 10.1583/JEVT-12-3861MR.1. [PubMed: 23210876]
- [26]. Han D, Kang SH, Kim SH, Yoon CH, Chae IH, Comparison of patency between two different peripheral self-expandable stents, absolute Pro[®] versus complete Se[®] in femoropopliteal occlusive disease, *Int. Angiol* 38 (2019) 305–311, doi: 10.23736/S0392-9590.19.04102-6. [PubMed: 31345007]
- [27]. Powell RJR, Jaff MR, Schroë H, Benko A, Diaz-Cartelle J, Müller-Hülsbeck S, Stent placement in the superficial femoral and proximal popliteal arteries with the innova self-expanding bare metal stent system, *Catheter. Cardiovasc. Interv* 89 (2017) 1069–1077, doi: 10.1002/ccd.26976. [PubMed: 28296239]
- [28]. Dake MD, Ansel GM, Jaff MR, Ohki T, Saxon RR, Smouse HB, Zeller T, Roubin GS, Burket MW, Khatib Y, Snyder S.a., Ragheb AO, White JK, Machan LS, Paclitaxel-eluting stents show superiority to balloon angioplasty and bare metal stents in femoropopliteal disease: twelve-month zilver PTX randomized study results, *Circ. Cardiovasc. Interv* 4 (2011) 495–504, doi: 10.1161/CIRCINTERVENTIONS.111.962324. [PubMed: 21953370]
- [29]. Marmagkiolis K, Hakeem A, Choksi N, Al-Hawwas M, Edupuganti MMR, Leesar MA, Cilingiroglu M, 12-month primary patency rates of contemporary endovascular device therapy for femoro-popliteal occlusive disease in 6,024 patients: beyond balloon angioplasty, *Catheter. Cardiovasc. Interv* 84 (2014) 555–564, doi: 10.1002/ccd.25510. [PubMed: 24740749]
- [30]. Gray WA, Feiring A, Cioppi M, Hibbard R, Gray B, Khatib Y, Jessup D, Bachinsky W, Rivera E, Tauth J, Patarca R, Massaro J, Stoll H-PP, Jaff MR, S.M.A.R.T., self-expanding nitinol stent for the treatment of atherosclerotic lesions in the superficial femoral artery (STROLL): 1-year outcomes, *J. Vasc. Interv. Radiol* 26 (2015) 21–28, doi: 10.1016/j.jvir.2014.09.018. [PubMed: 25454735]
- [31]. Garriboli L, Miccoli T, Pruner G, Jannello AM, PTA and stenting of femoropopliteal trunk with cordis smartflex stent system: a single-center experience, *Vasc. Endovasc. Surg* 54 (2020) 17–24, doi: 10.1177/1538574419875551.

- [32]. Badra A, Marques P, Braesco J, Albert B, Nasr B, Gouny P, One-year results of heavily calcified femoropopliteal artery stenting, *Inser. to Endovasc. Today Eur* 4 (2016) 23–25.
- [33]. Bishu K, Armstrong EJ, Supera self-expanding stents for endovascular treatment of femoropopliteal disease: a review of the clinical evidence, *Vasc. Health Risk Manag* 11 (2015) 387–395, doi: 10.2147/VHRM.S70229. [PubMed: 26203255]
- [34]. Cambiaghi T, Spertino A, Bertoglio L, Chiesa R, Fracture of a supra interwoven nitinol stent after treatment of popliteal artery stenosis, *J. Endovasc. Ther* 24 (2017) 447–449, doi: 10.1177/1526602817698655. [PubMed: 28351226]
- [35]. Valle JA, Famouri A, Rogers RK, Bend but don't break? A case of supra stent fracture in the popliteal artery, *J. Vasc. Endovasc. Surg* 02 (1:7) (2017) 1–4, doi: 10.21767/2573-4482.100039.
- [36]. Bosiers M, Setacci C, De Donato G, Torsello G, Silveira PG, Deloose K, Scheinert D, Veroux P, Hendriks J, Maene L, Keirse K, Navarro T, Callaert J, Eckstein HH, Te Berek J, Giaquinta A, Wauters J, ZILVERPASS study: ZILVER PTX stent vs bypass surgery in femoropopliteal lesions, *J. Endovasc. Ther* 27 (2020) 287–295, doi: 10.1177/1526602820902014. [PubMed: 31997715]
- [37]. Bisdas T, Beropoulos E, Argyriou A, Torsello G, Stavroulakis K, 1-Year all-comers analysis of the eluvia drug-eluting stent for long femoropopliteal lesions after suboptimal angioplasty, *JACC Cardiovasc. Interv* 11 (2018) 957–966, doi: 10.1016/j.jcin.2018.03.046. [PubMed: 29798772]
- [38]. Stavroulakis K, Torsello G, Bosiers M, Argyriou A, Tsilimparis N, Bisdas T, 2-Year outcomes of the eluvia drug-eluting stent for the treatment of complex femoropopliteal lesions, *JACC Cardiovasc. Interv* 14 (2021) 692–701, doi: 10.1016/j.jcin.2021.01.026. [PubMed: 33736776]
- [39]. Sakamoto A, Torii S, Jinnouchi H, Fuller D, Cornelissen A, Sato Y, Kuntz S, Mori M, Kawakami R, Kawai K, Fernandez R, Paek KH, Gadhoke N, Guo L, Kolodgie FD, Young B, Ragheb A, Virmani R, Finn AV, Vascular response of a polymer-free paclitaxel-coated stent (Zilver PTX) versus a polymer-coated paclitaxel-eluting stent (Eluvia) in healthy swine femoropopliteal arteries, *J. Vasc. Interv. Radiol* 32 (2021) 792–801.e5, doi: 10.1016/j.jvir.2021.02.014. [PubMed: 33677117]
- [40]. Cheng CP, Choi G, Herfkens RJ, Taylor CA, The effect of aging on deformations of the superficial femoral artery resulting from hip and knee flexion: potential clinical implications, *J. Vasc. Interv. Radiol* 21 (2010) 195–202, doi: 10.1016/j.jvir.2009.08.027. [PubMed: 20022767]
- [41]. Cheng C, Wilson N, Hallett R, *In vivo* MR angiographic quantification of axial and twisting deformations of the superficial femoral artery resulting from maximum hip and knee flexion, *J. Vasc. Interv. Radiol* 17 (2006) 979–987, doi: 10.1097/01.RVI.0000220367.62137.E8. [PubMed: 16778231]
- [42]. Nikanorov A, Smouse HB, Osman K, Bialas M, Shrivastava S, Schwartz LB, Fracture of self-expanding nitinol stents stressed *in vitro* under simulated intravascular conditions, *J. Vasc. Surg* 48 (2008) 435–440, doi: 10.1016/j.jvs.2008.02.029. [PubMed: 18486426]
- [43]. Nikanorov A, Schillinger M, Zhao H, Minar E, Schwartz LB, Assessment of self-expanding nitinol stent deformation after chronic implantation into the femoropopliteal arteries, *EuroIntervention* 9 (2013) 730–737, doi: 10.4244/EIJV9I6A117. [PubMed: 24169133]
- [44]. Ansari F, Pack LK, Brooks SS, Morrison TM, Design considerations for studies of the biomechanical environment of the femoropopliteal arteries, *J. Vasc. Surg* 58 (2013) 804–813, doi: 10.1016/j.jvs.2013.03.052. [PubMed: 23870198]
- [45]. MacTaggart JN, Phillips NY, Lomneth CS, Pipinos III, Bowen R, Timothy Baxter B, Johanning J, Matthew Longo G, Desyatova AS, Moulton MJ, Dzenis YA, Kamenskiy AV, Three-dimensional bending, torsion and axial compression of the femoropopliteal artery during limb flexion, *J. Biomech* 47 (2014) 2249–2256, doi: 10.1016/j.jbiomech.2014.04.053. [PubMed: 24856888]
- [46]. Vad S, Eskinazi A, Corbett T, McGloughlin T, Vande Geest JP, Determination of coefficient of friction for self-expanding stent-grafts, *J. Biomech. Eng* 132 (2010) 1–10, doi: 10.1115/1.4002798.

Statement of significance

Poor outcomes of peripheral arterial disease stenting are related to the inability of stents to accommodate the complex biomechanics of the flexed lower limb. Abrasion damage caused by rubbing of the stent against the artery wall during limb movement plays a significant role in reconstruction failure but has not been characterized. Our study presents the first attempt at assessing peripheral stent abrasiveness, and the proposed method is applied to compare the abrasion damage caused by Misago, AbsolutePro, Innova, Zilver, SmartControl, SmartFlex, and Supera peripheral stents using artery-mimicking synthetic tubes and cyclic deformations equivalent to five life-years of severe limb flexions. The abrasion damage caused by stents strongly correlates with their clinical 12-month primary patency and target lesion revascularization rates, and the described methodology can be used as a cost-effective and controlled way of assessing stent performance, which can guide device selection and development.

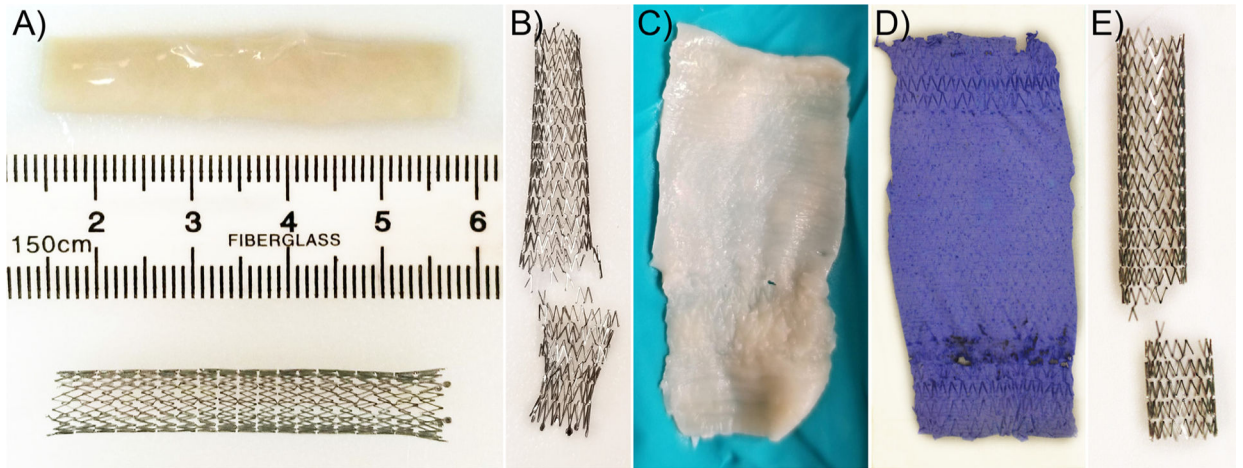


Fig. 1. (A) Human FPA with a deployed Smart Control stent, and (B) fractured stent that (C) penetrated the arterial wall after cyclic loading. Our nanofibrillar tube with the same stent design was able to reproduce the same results (D,E) but allowed the quantification of abrasion by analyzing the imprint of the stent on the tube wall (D).

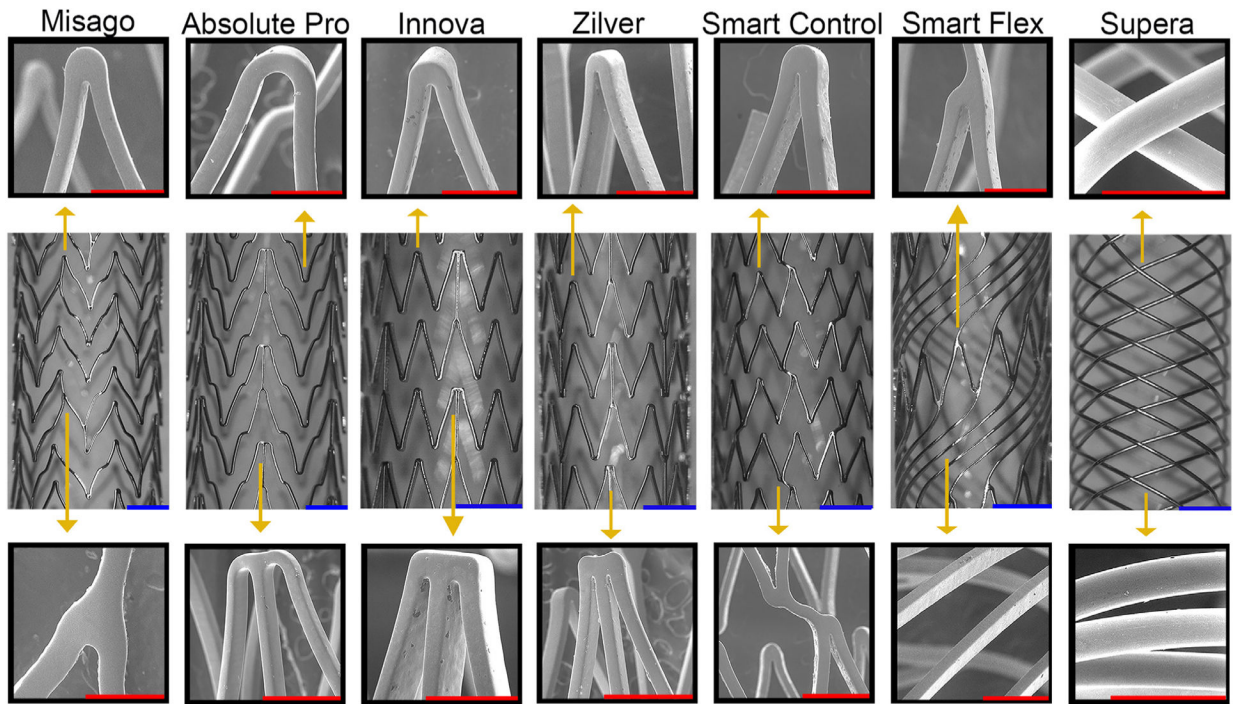


Fig. 2. Seven stent designs evaluated using scanning electron microscopy and demonstrating design features such as apexes and bridges that may contribute to abrasion. The red scale bar is 500 μm , and the blue scale bar is 2 mm.

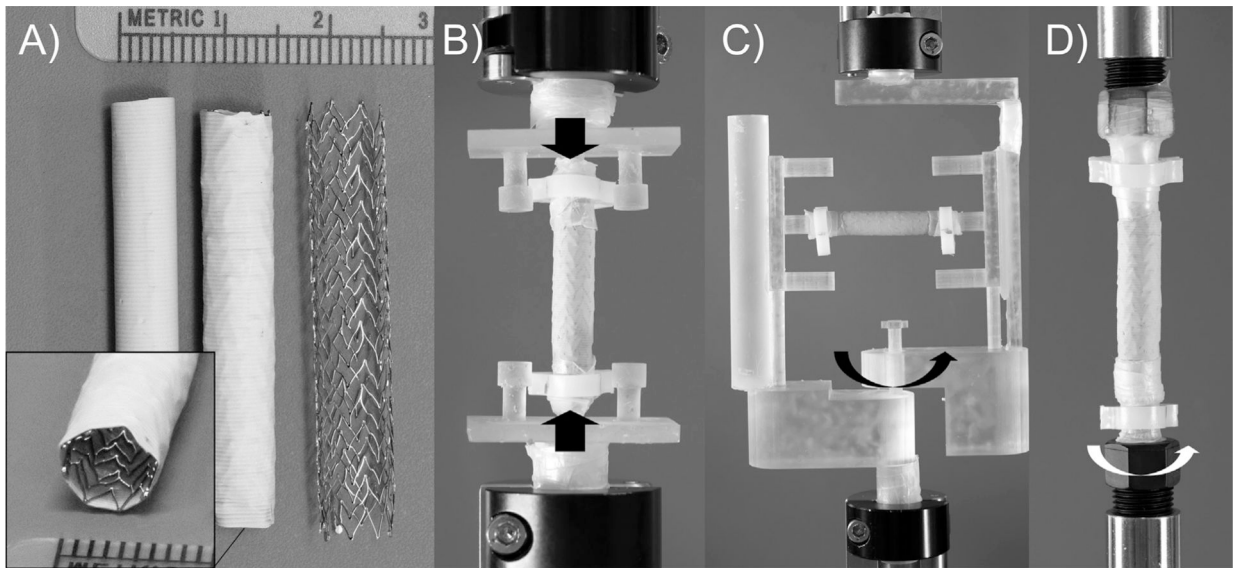


Fig. 3.
(A) Nanofibrous 6mm-diameter tube with a 7 mm Misago stent. Custom-made fixtures to subject the stents to (B) axial compression, (C) bending, and (D) torsion deformations.

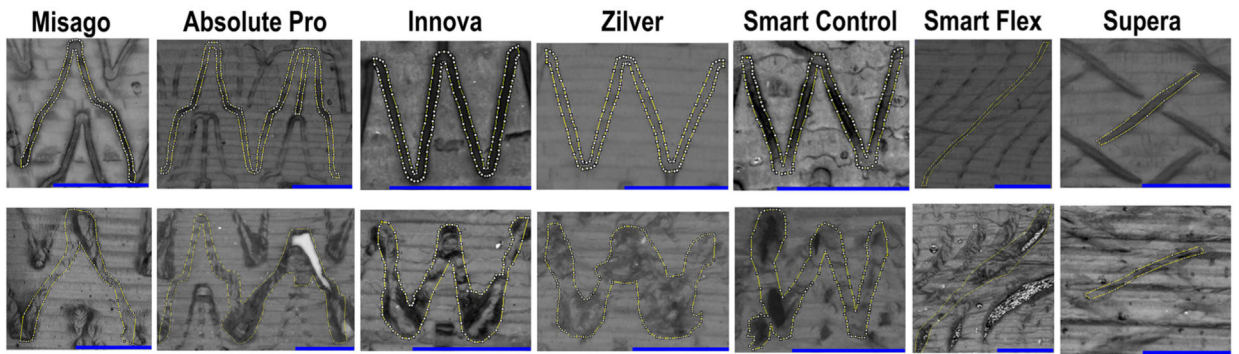


Fig. 4. Imprints of the non-abraded (top) and abraded (bottom) nanofibrillar tubes by each of the stent designs. The blue scale bar is 2 mm.

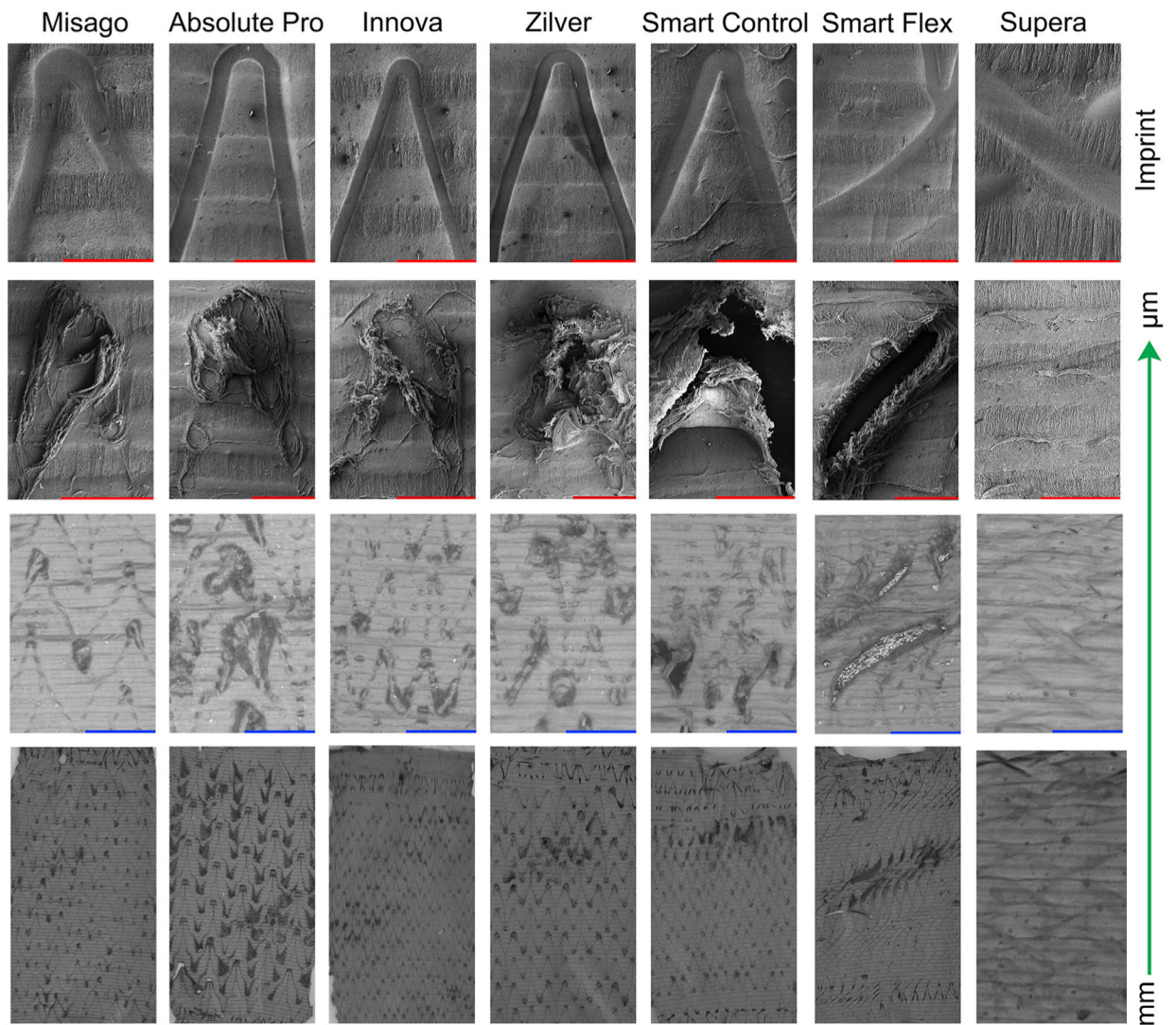


Fig. 5. Stent abrasion under cyclic axial compression. The top row demonstrates stent imprints, and the images below represent the abrasion areas at different scales, from μm to mm . The red and blue scale bars are $500\ \mu\text{m}$ and $2\ \text{mm}$, respectively.

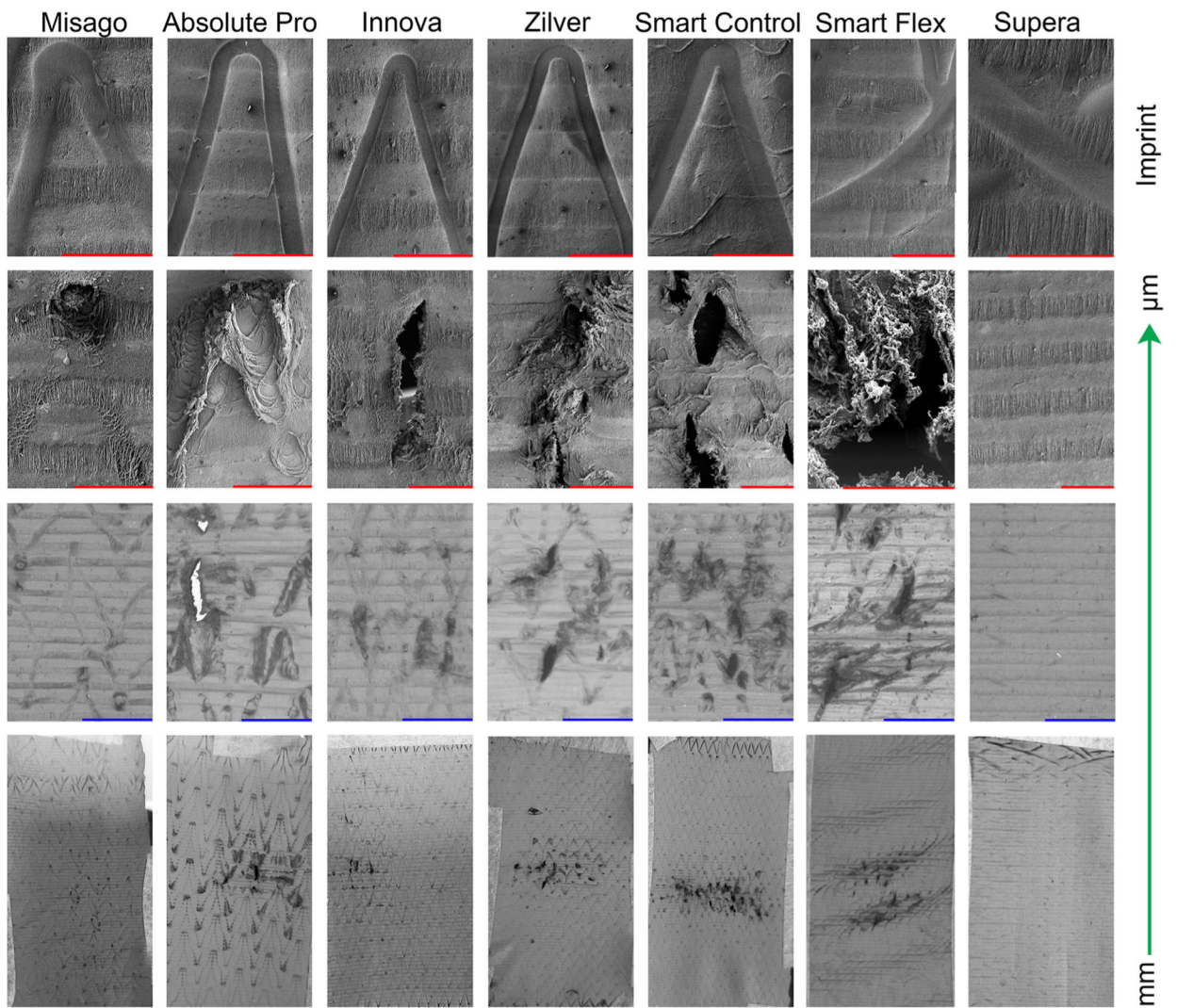


Fig. 6. Stent abrasion under cyclic bending. The red and blue scale bars are 500 μm and 2 mm, respectively.

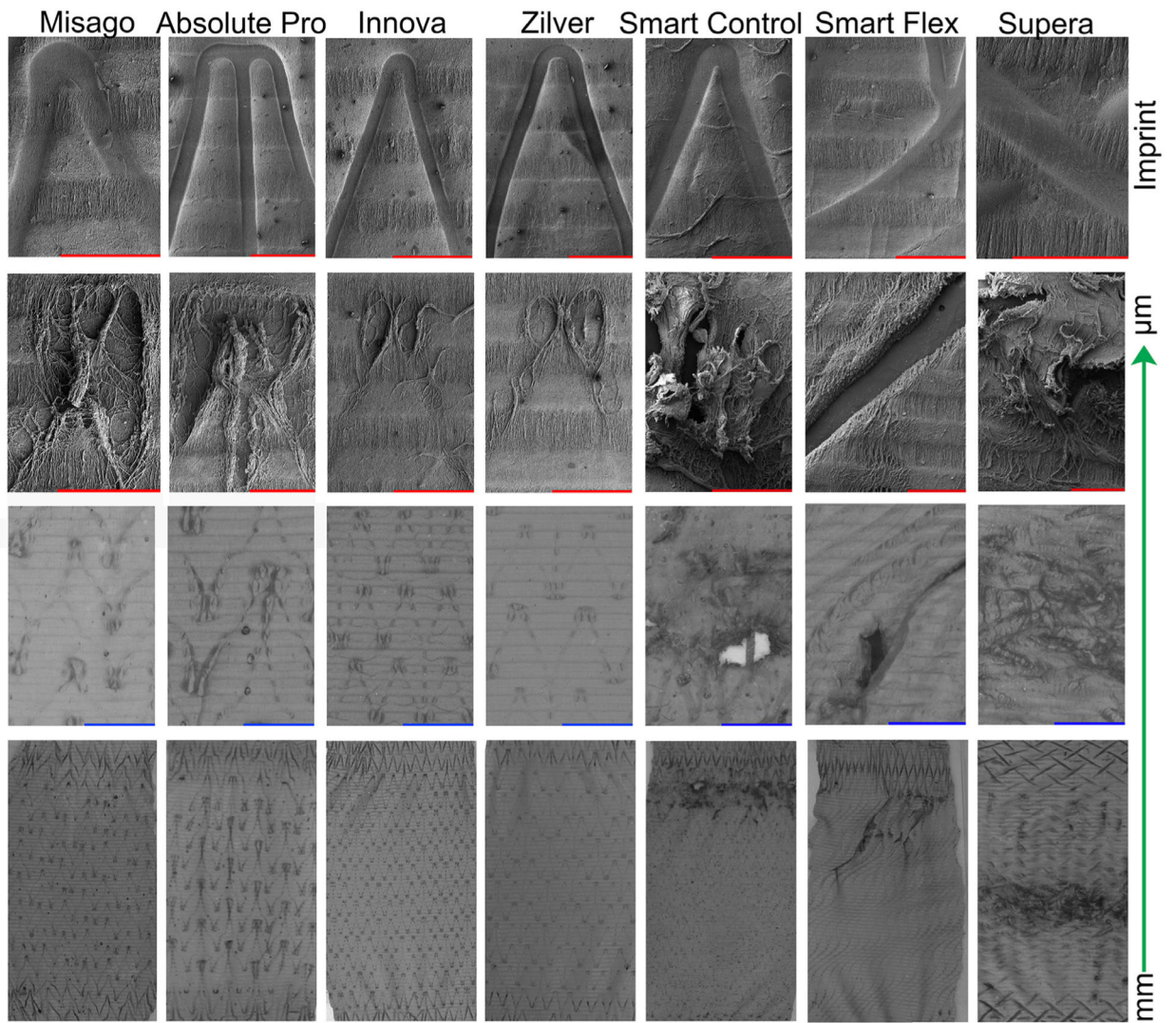


Fig. 7. Stent abrasion under cyclic torsion. The red and blue scale bars are 500 μm and 2 mm, respectively.

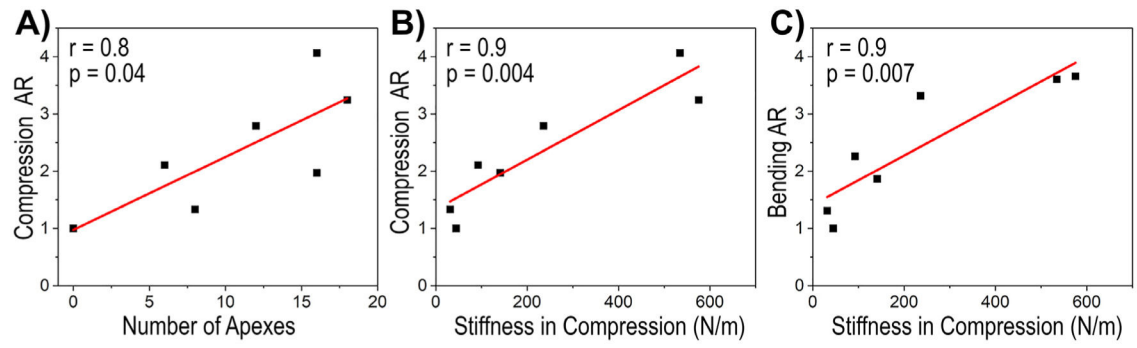


Fig. 8. Significant correlations between the Abrasion Ratio (AR) and stent design characteristics.

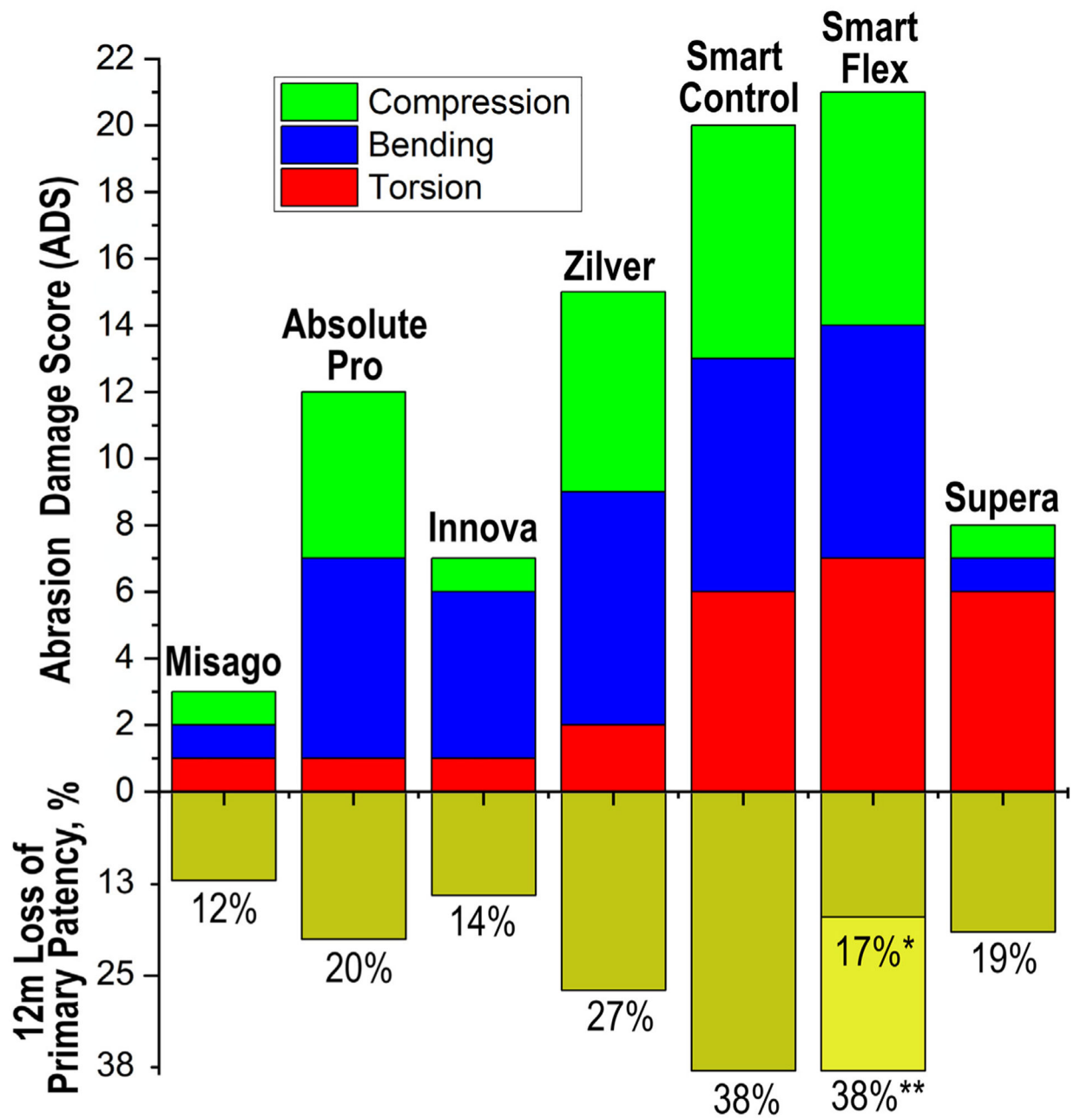









Fig. 9. Cumulative ADS and 12-month loss of primary patency (see Table 1).

Table 1

Stent strut profile characteristics, device stiffness [6], abrasion ratios (ARs), and abrasion damage scores (ADS). In the strut profile, the inner fillet (round corner) is on top.

	Misago	Absolute Pro	Innova	Zilver	Smart Control	Smart Flex	Supera
Strut Profile							
Thickness (µm)	198 ± 3	198 ± 7	221 ± 3	203 ± 1	202 ± 2	188 ± 3	176 ± 2
Width (µm)	103 ± 6	132 ± 11	93 ± 2	104 ± 2	104 ± 2	109 ± 2	176 ± 2
Inner Fillet (µm)	32 ± 2	41 ± 4	28 ± 1	29 ± 2	31 ± 1	26 ± 1	88 ± 1
Outer Fillet (µm)	38 ± 1	46 ± 4	31 ± 1	38 ± 1	36 ± 2	29 ± 2	88 ± 1
Apex Fillet (µm)	145 ± 3	236 ± 3	122 ± 2	114 ± 5	132 ± 3	167 ± 6	-
No. of Apexes	8	6	16	12	18	16	-
Stent Stiffness [6]							
Compression (N/m)	31	92	141	236	575	534	45
Bending (N/m)	10	17	33	40	98	54	32
Torsion (N/m)	16	9	23	19	86	66	959
Abrasion Ratio							
Compression	1.33 ± 0.25	2.11 ± 0.16	1.97 ± 0.28	2.79 ± 0.69	3.25 ± 0.93	4.07 ± 0.41	1 ± 0
Bending	1.31 ± 0.11	2.26 ± 0.72	1.86 ± 0.39	3.31 ± 0.69	3.65 ± 1.69	3.60 ± 0.81	1 ± 0
Torsion	1.40 ± 0.04	1.62 ± 0.02	1.82 ± 0.16	1.42 ± 0.04	2.61 ± 0.64	4.18 ± 1.18	2.47 ± 0.59

Author Manuscript

Author Manuscript

Author Manuscript

Author Manuscript

	Misago	Absolute Pro	Innova	Zilver	Smart Control	Smart Flex	Supera
Abrasion Damage Score	1	5	1	6	7	7	1
Compression	1	6	5	7	7	7	1
Bending	1	1	1	2	6	7	6
Torsion	1	12	7	15	20	21	8
Cumulative	3	80 [26]	86 [27]	73 [28]	62 [29,30]	83* [31]/62** [32]	81 [33]
12-month Primary Patency, %	88 [25]	80 [26]	86 [27]	73 [28]	62 [29,30]	83* [31]/62** [32]	81 [33]



*Assisted patency.
 **Freedom from target lesion revascularization (TLR).